

Climate responses to volcanic eruptions assessed from observations and CMIP5 multi-models

Seungmok Paik¹ · Seung-Ki Min¹

Received: 29 December 2015 / Accepted: 6 April 2016 / Published online: 15 April 2016
© Springer-Verlag Berlin Heidelberg 2016

Abstract This study analyzes climate responses to four volcanic eruptions that occurred since 1960s using observations (including reanalyses) and CMIP5 multi-model simulations. Changes in surface air temperature, specific humidity, and precipitation over the global land are examined during pre- to post-eruption years using a composite analysis. Observations exhibit consistent decreases in temperature, humidity, and precipitation following eruptions, which are reasonably captured by CMIP5 multi-models simulated including volcanic forcing. The observed and simulated decreases in temperature and humidity are stronger than the internal variability ranges (estimated from pre-industrial control simulations), indicating robust responses. On the other hand, the observed precipitation decrease is significant but the CMIP5 models considerably underestimate it, as reported by previous studies. In order to explore important physical processes determining climate responses to volcanic forcing, a surface energy budget is analyzed together with inter-model relationship between variables. A strong inter-model correlation ($r = 0.89$) appears between temperature and humidity, representing the Clausius–Clapeyron relation. Interestingly, precipitation is found to be closely related with latent heat flux ($r = -0.50$) and vertical motion (ω) at 500 hPa level ($r = -0.68$), changes of which are also underestimated by models. Further, by comparing estimates of precipitation minus evaporation between land and ocean, which is significantly correlated with vertical motion ($r = -0.73$), it is found that monsoon

circulation weakens after volcanic eruptions but CMIP5 models substantially underestimate it. Our results suggest that this dynamic response via monsoon circulation weakening can be a critical factor for models' underestimation of precipitation reduction to volcanic forcing.

Keywords Volcanic eruptions · CMIP5 models · Temperature · Precipitation · Surface energy budget · Vertical motion · Monsoon circulation

1 Introduction

Influence of tropical volcanic eruptions on global-scale temperature has been widely studied. Explosive volcanic eruptions emit sulfur dioxide gas to the stratosphere, which is oxidized to sulfate aerosols within a few weeks. In case of low latitude eruptions, aerosols tend to spread out globally and usually remain approximately for 1 year in the stratosphere (Lambert et al. 1993; Baran and Foot 1994; Barnes and Hofmann 1997). In the stratosphere, sulfate aerosols scatter incoming solar radiation, reducing the energy inflow in the earth's surface. As a result, surface temperature decreases for 2–3 years following volcanic eruptions (Robock and Mao 1995). On the other hand, sulfate aerosols absorb near infrared and terrestrial radiation, which induces warming in the lower stratosphere. The enhanced pole-to-equator temperature gradient is suggested to produce a positive North Atlantic Oscillation (NAO) like pattern, inducing anomalously warm surface air temperature over the northern hemisphere continents in the boreal winter (Robock 2000). This indirect winter warming response following eruptions has rather low signal-to-noise ratio, making a delicate change in the probability (Kodera 1994; Kirchner et al. 1999; Fischer et al. 2007; Hegerl et al. 2011).

✉ Seung-Ki Min
skmin@postech.ac.kr

¹ School of Environmental Science and Engineering, Pohang University of Science and Technology, Pohang, Gyeongbuk 37673, Korea

Evaluation studies show that CMIP5 models can reproduce surface cooling and stratospheric warming reasonably well (Driscoll et al. 2012; Flato et al. 2013) but generally fail to capture the dynamical response in the northern hemisphere following the eruptions (Driscoll et al. 2012). Several studies have analyzed hydrological cycle changes to volcanic forcing. In global terrestrial and several regions, precipitation decrease is identified in several observational studies (Gillett et al. 2004; Trenberth and Dai 2007). Recently, Iles and Hegerl (2015) detected the influence of volcanic eruptions on world major river flows. In terms of mechanisms, Bala et al. (2008) suggested that precipitation reduction is generated from evaporation or latent heat decrease and stabilized atmosphere after volcanic eruptions. With solar radiation increase experiment, Cao et al. (2012) suggested similar processes in opposite signs.

Also, recent studies (Peng et al. 2010; Joseph and Zeng 2011; Cao et al. 2012; Wegmann et al. 2014) suggested that the weakening of monsoon wind and circulation in boreal and austral summers is associated with the precipitation reduction due to disparity of heat capacity between land and ocean. Further, Joseph and Zeng (2011) suggested that different mechanisms exist over land and ocean. Using HadCM3 simulations and observational land precipitation datasets, Iles et al. (2013) found that climatologically wet regions experience drying in post-eruption years while dry regions become wetter. They also found model's underestimation in precipitation reduction during boreal winter, which originates from wet tropical regions. Using CMIP5 multi-model simulations, Iles and Hegerl (2014) reaffirmed the main features of precipitation responses and model underestimation.

In this study, climate responses to volcanic eruptions are further examined using observations (or reanalyses) and CMIP5 multi-model simulations. Particularly, we explore important factors responsible for models' weaker responses in precipitation reduction to volcanic eruptions. For this, a surface energy budget and vertical motion are analyzed and inter-model relationship is examined between climate variables and energy budget components. Also, we investigate monsoon weakening and order of responses between precipitation and latent heat over land and ocean to confirm mechanisms proposed by previous studies (Joseph and Zeng 2011) using multiple climate models.

In addition to multi-model analyses of mechanisms, this study employs advanced ways of estimating the signal of volcanic response and the noise of natural internal variability. Firstly, in order to better identify volcanic influence on climate in isolation, usually influences of the El Niño-Southern Oscillation (ENSO) should be removed (Santer et al. 2014) before analysis. Here we demonstrate

the importance of ENSO removal by comparing coupled model responses with those from atmospheric models integrated with the prescribed observed sea surface temperature (SST) condition (AMIP5 experiments). And then we remove ENSO influences from observations and models in a consistent manner. Secondly, since significance of climate responses to volcanic forcing should be tested against the natural variability noise ranges, methods of noise estimates can importantly affect results (Santer et al. 2014). As a rigorous way, here CMIP5 pre-industrial control simulations are used to estimate the ranges of internal climate variability.

Section 2 describes observed and simulated datasets as well as analysis methods. Results are explained in Sect. 3 including details of ENSO signal removal, composite analysis, surface energy budget analysis, vertical motion response, and monsoon flow changes. Conclusions and discussion are given in Sect. 4.

2 Data and analysis methods

2.1 Observations and reanalyses

The HadCRUT4 is used as surface temperature observations, which is a combined dataset of CRUTEM4 surface air temperature over land (Jones et al. 2012) with sea surface temperature of HadSST (Kennedy et al. 2011a, b) and available from 1850 to present. For precipitation observations, Global Historical Climatology Network's (GHCN) version 2 dataset (Peterson and Vose 1997) is used, which is available since 1900. Both datasets are monthly means on the resolution of $5^\circ \times 5^\circ$. In order to consider different space-time data availability between HadCRUT4 and GHCN dataset and obtain consistent and reliable responses, analysis is confined to grids where both observations exist for at least 70 % records during the actual analysis period (1958–1998, see below).

The twentieth Century version 2 (20CRv2) reanalysis dataset (Compo et al. 2011) is used to estimate the observed responses in specific humidity, shortwave and longwave radiations, and heat fluxes at the surface, vertical air temperature, and 500 hPa vertical motion (ω). Surface variables are provided on the resolution of 1.875° longitude \times $\sim 1.9^\circ$ latitude, and atmospheric variables are on $2^\circ \times 2^\circ$ grids. In order to test robustness of the results from 20CR reanalysis, we also use ERA40 reanalysis (Uppala et al. 2005, $2.5^\circ \times 2.5^\circ$ resolution) and compare results. All reanalysis data are interpolated onto $5^\circ \times 5^\circ$ grids and masked with the space-time data availability of the temperature and precipitation observations (see above).

Table 1 List of CMIP5 model simulations used in this study

Model	ALL	NAT	AMIP	CTL (no. of 62-year chunks)
ACCESS1.0				4
ACCESS1.3	1		1	8
BCC-CSM1.1	1	1	1	8
BCC-CSM1.1(m)	1		1	6
CCSM4	1	1	1	16
CESM1(BGC)	1			8
CESM1(CAM5)	1	1	1	5
CESM1(FASTCHEM)	1			3
CESM1(WACCM)	1			3
CNRM-CM5	1	1	1	13
CNRM-CM5-2	1			5
CSIRO-Mk3.6.0	1	1	1	
CanESM2	1	1		16
FGOALS-g2	1	1	1	11
FGOALS-s2				8
GFDL-CM3	1	1	1	
GFDL-ESM2G	1			
GFDL-ESM2 M	1	1		
GISS-E2-H	1	1		12
GISS-E2-H-CC	1			4
GISS-E2-R	1	1	1	13
GISS-E2-R-CC	1			4
HadCM3	1			
HadGEM2-CC				3
HadGEM2-ES	1	1		
INM-CM4	1		1	8
IPSL-CM5A-LR	1		1	6
IPSL-CM5A-MR	1	1	1	4
IPSL-CM5B-LR	1		1	4
MIROC-ESM	1	1	1	10
MIROC-ESM-CHEM	1	1		4
MIROC4 h	1			1
MIROC5	1		1	10
MRI-CGCM3	1	1	1	8
MRI-ESM1	1			
NorESM1-M	1	1	1	8
NorESM1-ME	1			4
Total	34 models	17 models	18 models	30 models (217 chunks)

Numbers of simulations are shown for ALL, NAT and AMIP. For CTL (preindustrial control), numbers of 62-year chunks are provided

2.2 CMIP5 data

We use multi-model datasets of the Coupled Model Intercomparison Project Phase 5 (CMIP5, Taylor et al. 2012) from historical (ALL, natural-plus-anthropogenic forcing), historicalNat (NAT, natural forcing only), AMIP5 and preindustrial control (pi-Control, CTL) experiments. For each experiment, single

ensemble member (r1i1p1, a first realization of the first version of the perturbed physics model) is used from each model, which provides all variables analyzed in this study. There are 34 models for ALL, 17 models for NAT, 18 models for AMIP5, and 30 models for CTL (see Table 1 for details of model list). From CTL runs, 217 non-overlapping 62-year chunks are extracted and 5–95 % range of the samples are defined as the noise of

Table 2 Information of major low latitude volcanic eruptions since 1960s analyzed in this study

Volcanoes	Eruption date	Latitude	Lower stratosphere SO ₂ mass (Tg)	El Niño years ^a	La Niña years ^a
Agung	Mar 17, 1963	8.34°S	20	1963–1964 1965–1966	1964–1965
Fuego	Oct 10, 1974	14.47°N	4		1973–1974 1974–1976
El Chichón	Apr 4, 1982	17.36°N	7	1982–1983	1984–1985
Pinatubo	Jun 15, 1991	15.13°N	20	1991–1992	

El Niño and La Niña years around each eruption are also provided

^a El Niño and La Niña years in post-eruption 3 years, obtained from the Climate Prediction Center in NOAA (http://www.cpc.noaa.gov/products/analysis_monitoring/ensostuff/ensoyears.shtml)

natural internal variability for each variable. All model data are interpolated onto the common 5° × 5° grid and masked with the observed data coverage prior to analysis.

2.3 Volcanic events and epoch analysis

This study analyzes four explosive low-latitude volcanic eruptions since 1960s (Table 2). Since these volcanoes are erupted at low latitudes, they are proper to study global impacts (Trepte and Hitchman 1992; Robock 2000). Also, more reliable observations are available to examine global responses for the recent period. Table 2 lists each volcano's information obtained from Bluth et al. (1997), Andres and Kasgnoc (1998), and Stothers (2001).

As in previous studies (Driscoll et al. 2012; Iles et al. 2013), epoch analysis is used to minimize low frequency natural variability in the volcanic responses. On grid base, relative responses are calculated with respect to pre-eruption 5-year means in each volcanic event. Following Iles et al. (2013), we require data to exist at least for 2 years over the 5 years in each month for calculating the pre-eruption means. Thereafter, four responses to volcanic eruptions are averaged to obtain composites. For AMIP experiments and associated comparisons, only two volcanoes (El Chichón and Pinatubo) are composited due to its limited simulation period (1979–2008, Taylor et al. 2012). In CTL experiment, each non-overlapping 62-year chunk is considered as the period of 1950–2011 and all calculation is done in the same way as for observations. For epoch analysis, changes from year −4 (4 years before) to year +7 (7 years after) relative to each eruption year are analyzed, and year +1 is defined as 12-month average since 4 months pass following the eruption dates (Table 2).

3 Results

3.1 ENSO influence removal

ENSO exerts large impacts on global temperature and precipitation patterns for a few years (Halpert and Ropelewski

1992; Gu et al. 2007; Liu et al. 2012). Most recent volcanoes (Table 2) occurred during El Niño periods, so volcanic signals could be contaminated by ENSO influences. In fact, there have been some debates on whether the volcanic eruptions trigger the ENSO or not. Adams et al. (2003) suggested that volcanic eruptions could increase possibility of ENSO genesis using palaeoclimate reconstruction datasets. Also, several studies found an increased ENSO probability after volcanic eruptions from model simulation results (Mann et al. 2005; Emile-Geay et al. 2008; Maher et al. 2015). On the other hand, Self et al. (1997) insisted that volcanic eruptions and outbreak of ENSO do not have a co-relationship. For simplicity, we assume that there is no connection between volcanic eruptions and occurrence of ENSO.

In order to assess ENSO influence, we compare temperature and precipitation responses averaged over the global land to two recent volcanoes using ALL and AMIP simulations from 18 common models for 1979–2005 (Table 1). Figure 1 shows results. ALL runs show cooling and drying for 2–3 years after eruptions with maximum responses at the year +1. In contrast, AMIP results obtained from the same models but under the observed SST conditions display much weaker cooling but much stronger drying responses than ALL results at the year +1, suggesting strong influence of the observed SST patterns and ENSO events on these estimated composite responses. When removing ENSO signals from AMIP runs based on linear regression (see below for detailed method), temperature and precipitation responses become remarkably similar to those from ALL runs. This clearly indicates that ENSO can disturb volcanic signals and its influence needs to be removed for examining volcanic signals in isolation when particularly analyzing single SST-based results like AMIP and observations.

We use the Niño3.4 index to represent the observed ENSO, which is defined as area-averaged SST anomalies in the Niño3.4 region (5°S–5°N, 120°W–170°W). Using the Niño3.4 index, we remove ENSO influence from the observations following the method used in Santer et al. (2001). Firstly, a month of maximum regression coefficient is searched for between area-averaged data and the Niño3.4

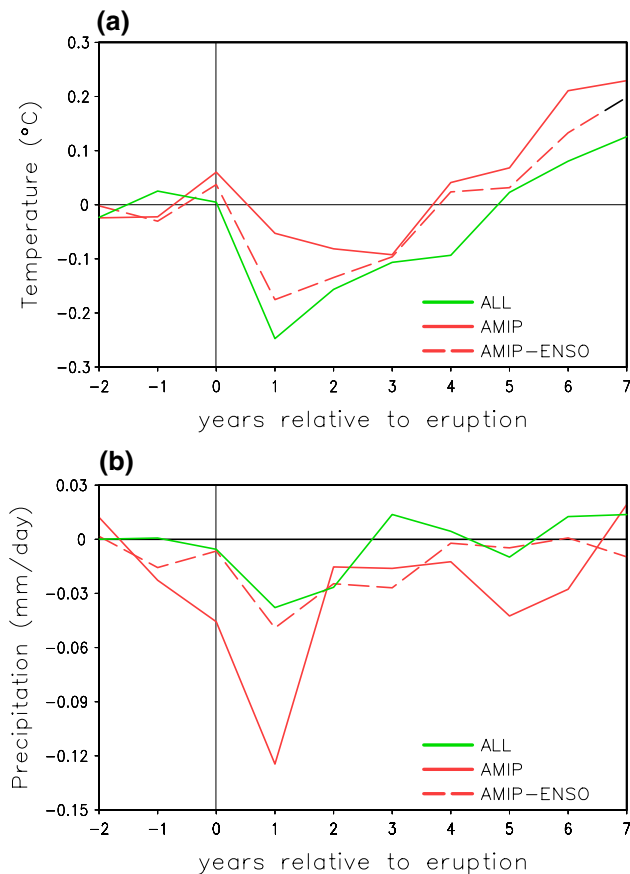


Fig. 1 Multi-model mean global land averaged responses of **a** temperature and **b** precipitation to El Chichón and Pinatubo eruptions from ALL (green solid), AMIP (red solid) and ENSO-removed AMIP (AMIP-ENSO, red dashed) simulations. 18 models that provide both AMIP and ALL runs are used

index during 1951–2010 with applying a maximum lead or lag of 12 months (Note that the correlation between area-averaged data and the Niño3.4 index is generally maximized at the same lag as the regression coefficient). Next, for the selected month of maximum lag regression coefficient, ENSO signal is regressed out from gridded data. This procedure of finding maximum lag regression coefficient and removing ENSO signals is repeated ten times. In AMIP experiment, due to its short period, ENSO influence is removed with the same method but using 1979–2005 (see above and Fig. 1). For the CTL experiment, given each 60-year chunk (see above), ENSO influence is regressed out using the corresponding Niño3.4 index obtained from the sample with applying same lag or lead months as used in observations for each variable. All results below for observations (including reanalyses) and CTL simulations are based on ENSO-removed datasets. However, for ALL and NAT experiments, ENSO influences are not removed from each model because here multi-model ensemble mean (MME) is used to estimate climate responses to external

forcing as in previous studies (e.g., Iles and Hegerl 2014). Taking MME across many models will cancel out large part of different ENSO influences, which arise from chaotic internal variability due to freely driven air-sea coupling in each model. Therefore, final MME will show smoother responses to external forcing (cf. Flato et al. 2013).

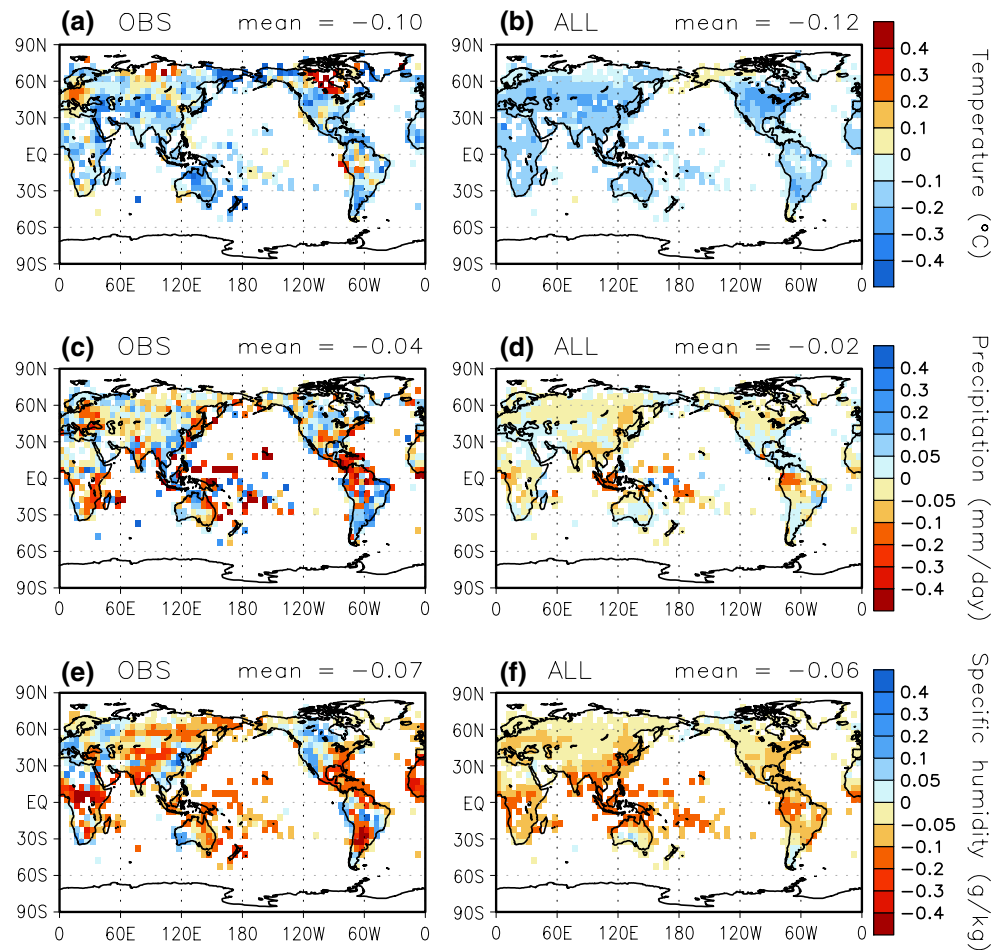
3.2 Volcanic signal patterns

Figure 2 illustrates spatial patterns of temperature, precipitation, specific humidity responses to volcanic eruptions from observations (20CR reanalysis for humidity), and ALL MMEs, which are averages for three post-eruption years. Overall cooling and drying are dominant for both observations and ALL. The observed response shows relatively heterogeneous patterns with sporadic responses, especially for precipitation reduction, which is concentrated on tropics. But in global land averages, cooling and drying signal is apparent with 0.10 K surface cooling, 0.04 mm/day drying, and 0.07 g/kg specific humidity decrease, respectively (Fig. 2). ALL MMEs provide spatially homogeneous responses with cooling and drying almost everywhere. Temperature response is stronger in mid-latitudes whereas precipitation and moisture responses are stronger in tropics than other regions. Simulated magnitudes of temperature and humidity responses are very similar to the observed. However, precipitation responses look much weaker than observations (about a half for global land mean), consistent with the model underestimation of precipitation reduction as reported by previous studies (Iles et al. 2013; Iles and Hegerl 2014). On the other hand, composite analysis for two post-volcanic winters shows that ALL MMEs cannot capture the observed winter warming responses over the high latitude continents (not shown), corroborating the finding of Driscoll et al. (2012).

Figure 3 shows observed (reanalysis for humidity) and ALL and NAT responses of global land averaged temperature, precipitation, and specific humidity to four volcanic eruptions. Although there are some differences in year of maximum response, temperature responses are similar between observations and ALL. NAT has greater cooling than ALL and observations, which is due to the omission of anthropogenic warming. Significance of volcanic signals can be tested against the internal variability ranges estimated as 5–95 % of CTL results (gray shading in Fig. 3) as done in previous studies (Gillett et al. 2004; Iles et al. 2013). During post-eruption 3 years, most cooling responses exceed the internal variability range, except for year +1 in the observations and year +3 in ALL. NAT temperature responses are much greater than internal variability during 3 years.

Precipitation responses from observation and CMIP5 experiments are shown in Fig. 3b. Although considerable

Fig. 2 Spatial patterns of observed (*left*) and multi-model mean ALL (*right*) post-eruption 3-year mean responses following four volcanic eruptions for **a, b** temperature, **c, d** precipitation and **e, f** specific humidity (from 20CRv2 reanalysis)



decreases appear in ALL and NAT experiments, precipitation responses from models are insignificant with MME amplitudes being located near to the lower bound (5th percentile) of the CTL noise. In contrast, observed reduction in precipitation is much stronger and beyond the noise range. This suggests that models underestimate the observed magnitude in precipitation reduction, matching well with Iles and Hegerl (2014). CMIP5 model responses during post-eruption 3 years are less than a half of the observed, and the observed reduction in precipitation appears longer up to year +4 after eruptions. Unlike temperature responses, ALL and NAT responses are very similar in amplitudes and temporal patterns, indicating that anthropogenic forcing does not induce robust long-term changes in global land precipitations during the analysis period (Gillett et al. 2004).

Responses of surface specific humidity, which are estimated from the 20CR reanalysis (Fig. 3c), resembles the temperature response. Surface moisture decreases on average over land during 3 years after eruption. After that, recovery occurs with a long-term moistening trend, which is due to anthropogenic warming as in the case of temperature. ALL shows largely similar responses to that

from reanalysis, reproducing the moisture decreases during 3 years and long-term increase after that. NAT results give larger and longer decreases in surface moisture than ALL. The observed and simulated signals of moisture reduction are found to be larger than the internal variability noise in most years except for year +3 in ALL.

3.3 Surface energy budget

Previous studies suggested that precipitation reduction is related to radiation and heat flux components (Bala et al. 2008; Cao et al. 2012). In this respect, surface energy budget is analyzed to further understand the model underestimation in precipitation reduction. Figure 4 shows surface radiation and heat flux responses at post-eruption years. The net-flux consists of net-longwave and net-shortwave radiations and latent and sensible heat fluxes. Note that positive signs represent downward direction in both radiation and heat fluxes. During two or three post-eruption years, net-shortwave radiation is reduced significantly in the 20CR reanalysis and ALL and NAT experiments with the greatest response at year +1, which is generated by aerosol optical depth increase

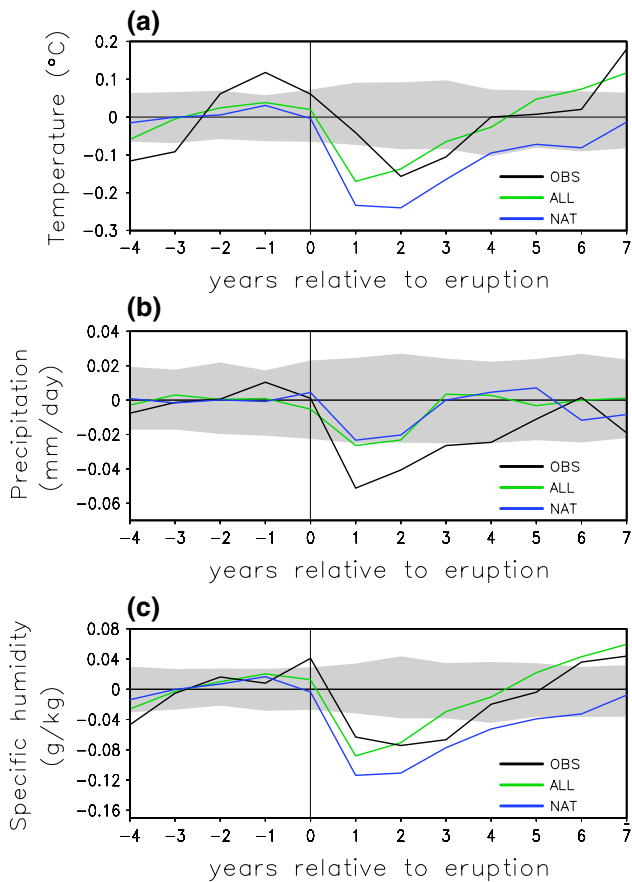


Fig. 3 Global land averaged annual mean responses of **a** surface temperature, **b** precipitation, **c** specific humidity to four eruptions from observations (reanalysis for humidity) and multi-model mean ALL and NAT simulations. *Gray shadings* indicate natural internal variability range estimated from CTL simulations

in the stratosphere. The decrease in downward shortwave radiation flux consequently perturbs longwave and heat fluxes. Due to comparable changes between up-welling and down-welling longwave radiation fluxes, significant change is not found in net-longwave radiation. On the other hand, in case of latent heat flux, the reanalysis and CMIP5 experiments exhibit significant (anomalous downward flux) increases during two or three post-eruption years. However, CMIP5 models tend to underestimate the increase in reanalysis. For 3-year averages, modeled responses in ALL and NAT are approximately two thirds of reanalysis. Similarly, significant (anomalous) increases in (downward) sensible heat flux occur at year +1 with similar intensity between reanalysis and models. As a result of radiation and heat flux perturbations, total net surface downward energy flux in the reanalysis is decreased significantly during year +1, which is well captured by ALL and NAT experiments. There are almost no differences in surface energy budget between ALL and NAT results, indicating negligible influence of

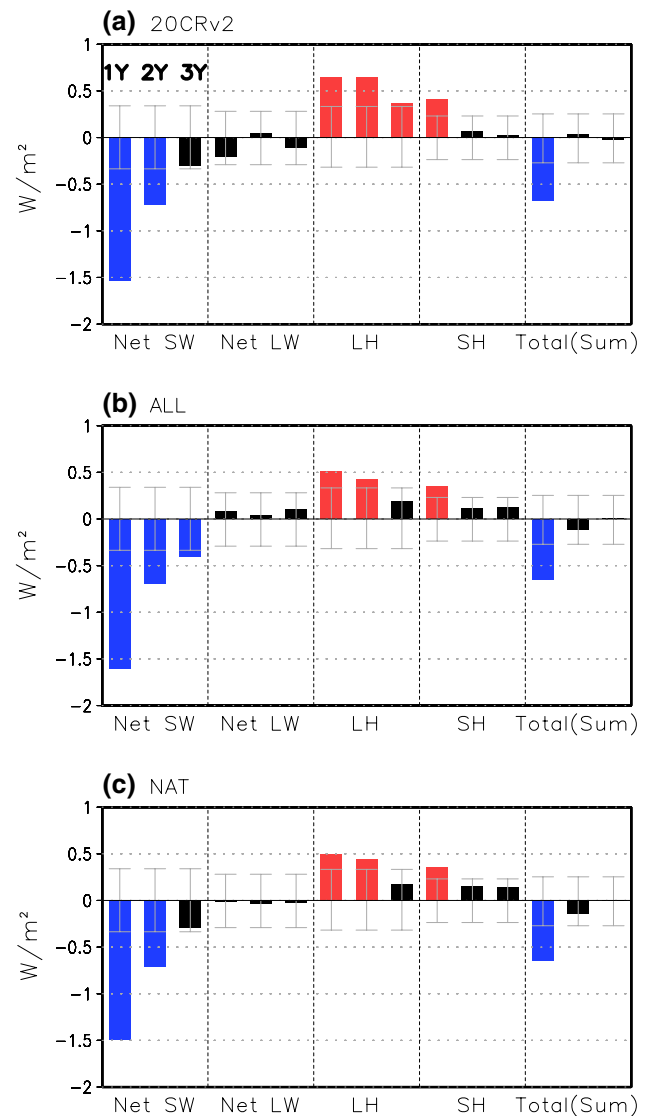


Fig. 4 Surface energy budget responses to four volcanic eruptions over land: changes in net shortwave (Net SW) and net longwave (Net LW) radiations, and latent heat (LH) and sensible heat (SH) fluxes during post-eruption 3 years obtained from **a** 20CRv2 reanalysis and **b** ALL and **c** NAT simulations. For each component, annual response from year +1 to year +3 is plotted from *left to right*. *Gray error bars* indicate natural variability ranges estimated from CTL. Reference direction is down-welling for all fluxes and total net flux is sum of all fluxes (Total = Net SW + Net LW + LH + SH)

anthropogenic warming on this short-term year-to-year responses.

To further analyze important factors determining climate responses, inter-model correlations between variables and surface energy flux components are examined using 34 ALL models for post-eruption 3-year mean values. Figure 5a illustrates that surface air temperature and specific humidity responses are highly correlated across models ($r = 0.89$; Table 3) and also that MME response

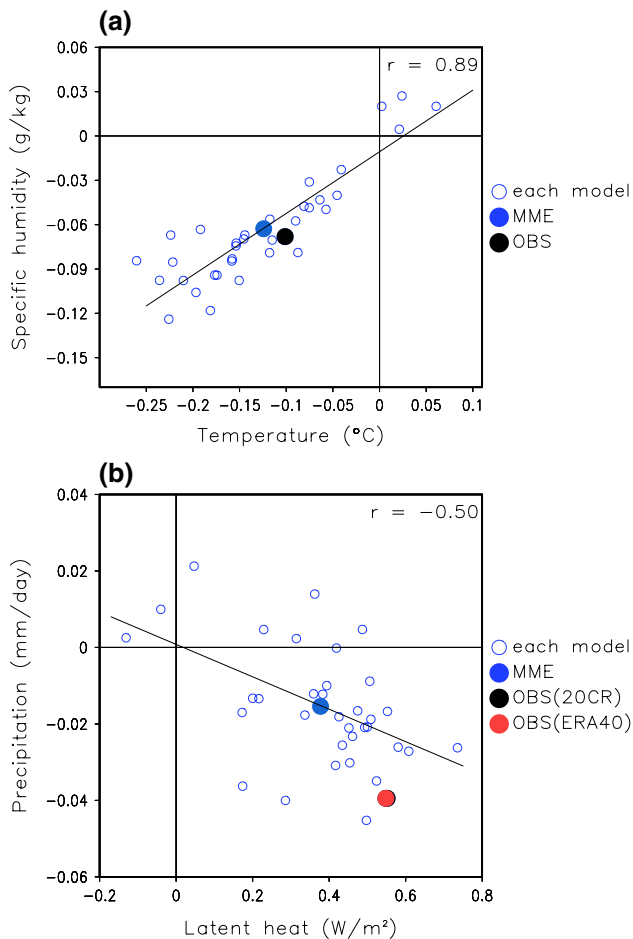


Fig. 5 Inter-model relationships **a** between surface air temperature and specific humidity, and **b** between latent heat and precipitation over land. Post-eruption 3-year mean values are plotted using each model ALL simulations (*blue open circles*) and multi-model mean (MME, *blue filled circle*) in comparison with observations (reanalyses for specific humidity and latent heat). Correlation coefficients calculated from 34 model values are presented

amplitude is very similar to the observed (reanalysis for humidity). This close inter-model relationship between temperature and moisture represents that model responses follow the Clausius–Clapeyron relation. That is, models with stronger cooling tend to have more reduction in moisture while models with less cooling tend to show less decrease in moisture at the surface. Also, these cooling and drying responses are found to be significantly correlated with shortwave, latent heat and net flux perturbations (Table 3).

Interestingly, precipitation is found to be highly correlated with latent heat flux ($r = -0.50$; Table 3). Figure 5b displays inter-model relationship between latent heat and precipitation from 34 CMIP5 models. Although it is less robust compared to the temperature-moisture association,

this link indicates the importance of latent heat changes in determining precipitation responses in the model. More importantly, many models underestimate increase in latent heat flux (downward direction) as they underestimate precipitation decreases after the volcanic events. We also examine this relationship using 2 years after eruption when CMIP5 models show significant precipitation reductions. Results are found to be essentially same as the 3-year mean results (not shown). The response of latent heat flux estimated from ERA40 reanalysis gives almost the same strength as that from 20CR, increasing the reliability of the latent heat response. In short, this robust result suggests that CMIP5 model underestimation of precipitation reduction is significantly related to weaker responses in the latent heat flux.

3.4 Vertical motion

As other factors in connection with precipitation responses, we examine changes in atmospheric stability and vertical motion. Atmospheric stability is measured by the vertical gradient of equivalent potential temperatures (θ_e) between 300 and 850 hPa levels, which are calculated from both 20CRv2 and ERA40 reanalyses. The atmospheric stability is found to increase following volcanic events from both reanalyses although some differences exist between two datasets (Fig. 6a). Generally, anomalous reduction in θ_e is greater in lower levels due mainly to more moisture reduction (not shown).

Response of atmospheric upwelling, which is physically consistent with atmospheric stability as well as precipitation, is examined using vertical motion (ω) at 500 hPa level (Fig. 6b). Both reanalyses show clear increases in ω (i.e., decrease in vertical motion) during year +1. Results from ALL experiments display some increases in 500 hPa ω , but its magnitude is much smaller than those from reanalyses. This underestimation is partly due to the large cancelation across models when taking MMEs, but it can be seen that most CMIP5 models underestimate the decrease in vertical motion (Fig. 6c). Even about half of models fail to capture the sign of the vertical motion change in reanalyses. Nevertheless, there is a strong inter-model correlation between 500 hPa vertical motion and precipitation responses. Using 3 year mean values following the events, a statistically significant relationship ($r = -0.68$) is obtained (Fig. 6c). Additionally, reanalysis values well follow the line of the inter-model relationship, supporting robustness of this relationship. The use of 2-year means does not affect results (not shown). Above results suggest that vertical motion, which is closely related to precipitation and atmospheric stability, can be critical factor in models' underestimation in precipitation reduction.

Table 3 Inter-model correlations between climate variables

	Surface air temperature	Precipitation flux	Specific humidity	Net SW	Net LW	LH	SH	Net flux	500 hPa ω	P – E
Surface air temperature	1	0.02	0.89	0.61	0.25	-0.45	-0.43	0.46	0.36	-0.19
Precipitation flux	0.02	1	0.14	0.17	0.13	-0.50	0.40	0.12	-0.68	0.91
Specific humidity	0.89	0.14	1	0.45	0.60	-0.57	-0.16	0.53	0.21	-0.10
Net SW	0.61	0.17	0.45	1	-0.28	-0.52	-0.58	0.52	0.23	-0.05
Net LW	0.25	0.13	0.60	-0.28	1	-0.31	0.44	0.30	-0.09	0.00
LH	-0.45	-0.50	-0.57	-0.52	-0.31	1	-0.12	-0.11	0.11	-0.10
SH	-0.43	0.40	-0.16	-0.58	0.44	-0.12	1	-0.07	-0.48	0.40
Net flux	0.46	0.12	0.53	0.52	0.30	-0.11	-0.07	1	0.11	0.08
500 hPa ω	0.36	-0.68	0.21	0.23	-0.09	0.11	-0.48	0.11	1	-0.73
P – E	-0.19	0.91	-0.10	-0.05	0.00	-0.10	0.40	0.08	-0.73	1

Correlation coefficient is calculated using post-eruption 3-year mean responses to volcanic forcing from 34 historical models (Table 1). Bold represents statistical significant correlations at 5 % level. SW and LW represent net shortwave and longwave flux at the surface while LH and SH depicts latent and sensible heat flux at the surface. P – E indicates precipitation minus evaporation at the surface

3.5 Monsoon flow

Following suggestions by previous studies (Joseph and Zeng 2011; Cao et al. 2012), we examine changes in monsoon circulation by looking at precipitation minus evaporation (P – E) averaged over land and ocean. 33 CMIP5 models (Table 1, except INMCM4) that provide land fraction data are used in this analysis. Grid cells having more than 25 % land fraction are defined as land (except for Antarctica) and the rest region is defined as ocean. First, as in Cao et al. (2012), P – E is analyzed to examine whether the monsoonal type flow changes or not after volcanic eruptions (Fig. 7b). Observed results are also compared with ALL results, for which the same observational coverage is applied to all 34 models (Fig. 7a). In accord with previous findings, land experiences freshwater deficit (P – E < 0) in both the observations and CMIP5 models (Fig. 7a, b). It is also found that CMIP5 models underestimate this response (Fig. 7a). In contrast, freshwater surplus (P – E > 0) occurs over ocean following volcanic eruptions. This means that mean water vapor transport from ocean to land is reduced, due to difference in heat capacity between them. Further, significant inter-model correlation ($r = -0.73$) is obtained between P – E and 500 hPa vertical motion over land (Fig. 7c). This relationship is physically reasonable since P – E means vertical moisture convergence (Trenberth et al. 2011). We estimate the amount of water vapor transport from ocean to land using ALL MMEs by calculating sum of P – E (E – P) over land (ocean). MME transport of ocean-to-land moisture ($42 \times 10^3 \text{ km}^3/\text{year}$) turns out to be very similar to the observed estimate (about $40 \times 10^3 \text{ km}^3/\text{year}$; Trenberth et al. 2011) also with a good balance between

land and ocean. Our estimation based on models suggests that volcanic eruptions on average reduce the total ocean-to-land water vapor transport by about 2 %.

To further understand the mechanisms related to precipitation reduction, we use a time marker following the method used in Joseph and Zeng (2011) using CMIP5 ALL experiments. Latent heat and precipitation are smoothed with a 12-month running-average after composites over four volcanoes and multi-model means are obtained for land and ocean, respectively. Figure 8a shows the results for land. It shows that precipitation reduction leads approximately 1 month to decrease in latent heat flux (note upward direction for better comparison) in land, consistent with what Joseph and Zeng (2011) found. This represents weakened monsoon type circulation that induces water vapor decrease in land atmosphere, which in turn makes precipitation reduction. As a result, latent heat flux is decreased in response to water deficit in the land. An interesting feature here is an excessive recovery of land precipitation in year +3, but this response seems very weak, lying within the internal variability ranges (not shown). In contrast to land responses, over ocean, latent heat flux decrease (upward) leads to precipitation reduction by around 1 month (based on the 1st peak), indicating that precipitation reduction is a response to latent heat flux change to volcanic forcing (Fig. 8b). This means that perturbation of surface latent heat or evaporation is more crucial than freshwater transport in the ocean. In terms of two peaks in precipitation response over ocean, further investigation is warranted in the future work. Additionally, maximum increase in 500 hPa ω (vertical anomalous downward motion) is found to occur concurrently with maximum precipitation reduction in land (not shown). Significant inter-model correlations between precipitation and latent heat or

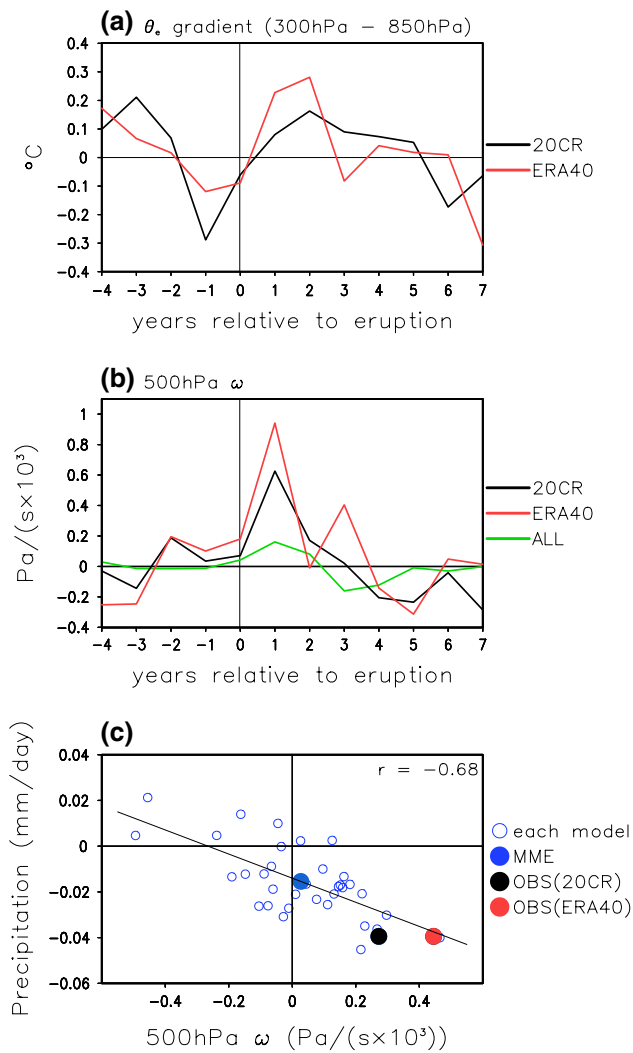


Fig. 6 Annual mean responses of **a** equivalent potential temperature gradient (300 – 850 hPa) and **b** 500 hPa ω over land to four volcanic eruptions, estimated from two reanalyses (20CRv2 and ERA40) and ALL simulations (only for 500 hPa ω), and **c** same as Fig. 5 but the inter-model relationship between 500 hPa ω and precipitation

between precipitation and 500 hPa ω are also identified in both land and ocean (not shown), confirming strong relationship between them (Table 3).

4 Conclusions and discussion

In this study, climate responses to four recent volcanic eruptions are examined using observations (including reanalyses) and CMIP5 multi-model simulations. During post-eruption years, global cooling and drying responses occur and precipitation reduction is concentrated in tropics. CMIP5 multi-model simulations including volcanic forcing are found to reproduce the observed reductions in

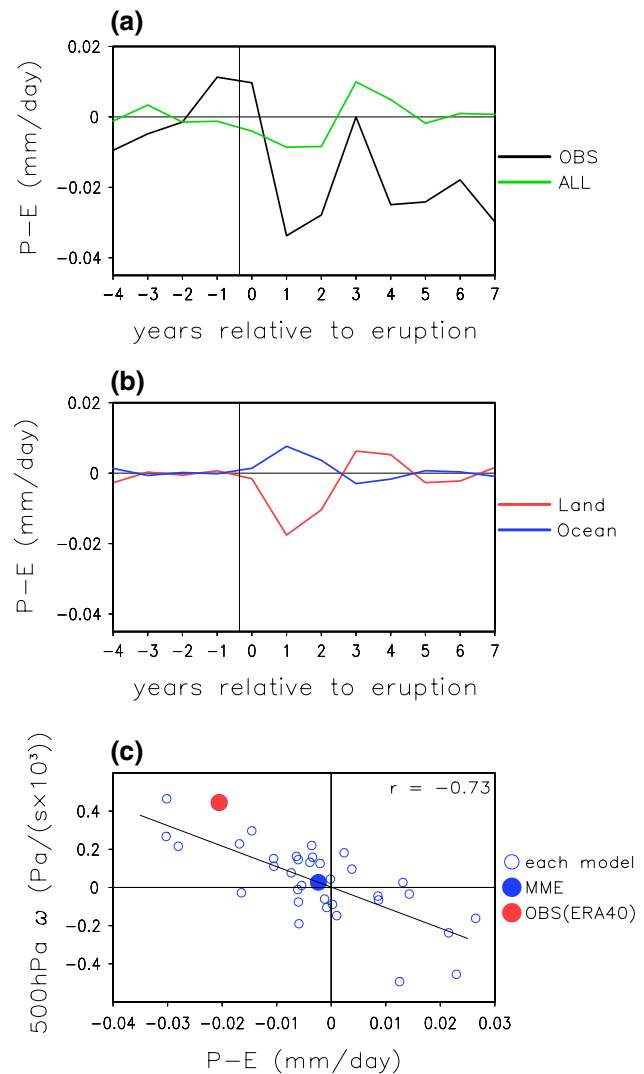
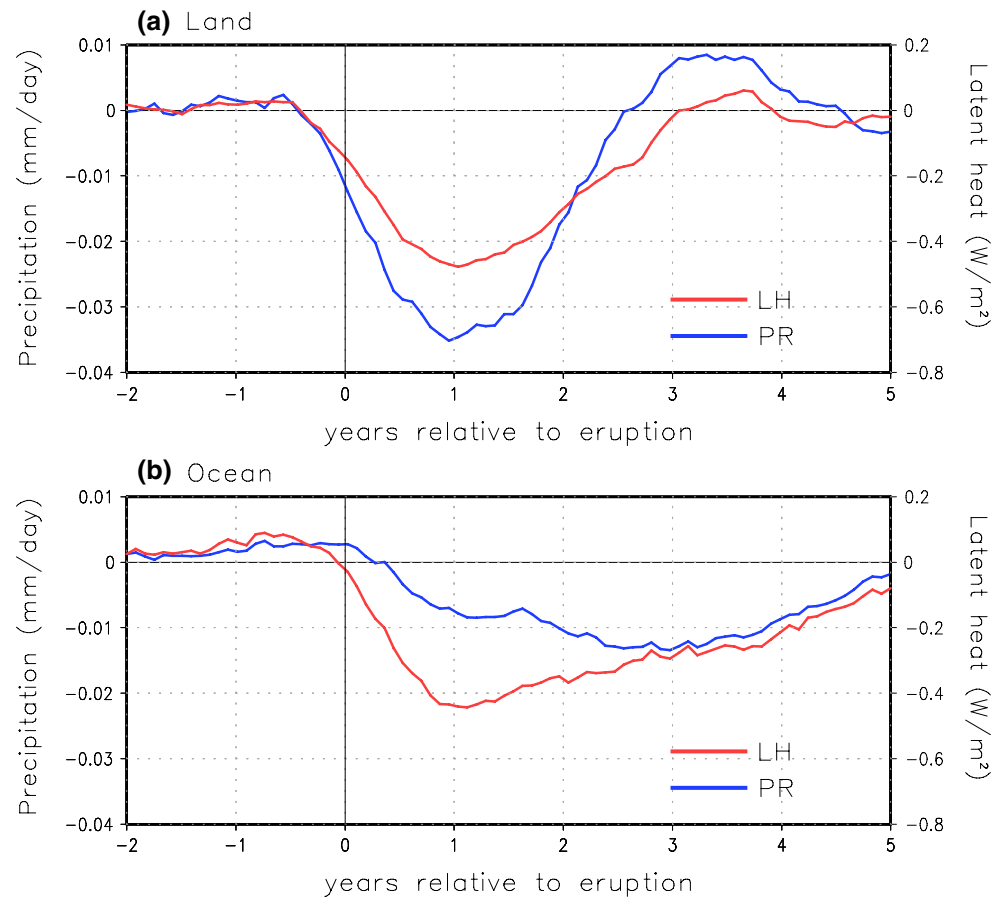


Fig. 7 **a** Precipitation minus evaporation (P – E) response in observation and ALL simulations for the observed spatial coverage, **b** P – E responses from ALL simulations over land (red) and ocean (blue), and **c** same as Fig. 5 but for the inter-model relationship between P – E and 500 hPa ω

temperature and humidity reasonably well, amplitudes of which are statistically significant beyond the ranges of natural internal variability. However, CMIP5 models generally underestimate the observed precipitation reduction, consistent with previous studies.

To explore factors associated with weaker precipitation reduction in CMIP5 models, a surface energy budget and vertical motion change to volcanic forcing and the inter-model relationship between components are examined. A very strong inter-model correlation is obtained between temperature and humidity reduction, indicating the Clausius–Clapeyron relation. Also, these cooling and drying responses are found to be related with net shortwave, latent heat and net flux perturbations (Table 3). It is demonstrated

Fig. 8 Latent heat (LH) and precipitation (PR) responses in **a** land and **b** ocean to four volcanic eruptions from ALL simulations. Results are smoothed with a 12-month running average, and the sign of LH flux responses (*positive* upward direction) is changed for better comparison with precipitation. Vertical black lines indicate the exact time of month when volcanoes erupted



that most CMIP5 models underestimate the latent heat flux increase (downward direction), which is significantly correlated with the precipitation reduction ($r = -0.50$). Further analysis shows that atmospheric stability increases after volcanic eruptions, supporting previous studies (Bala et al. 2008; Cao et al. 2012). Also, downward motion at 500 hPa exhibits anomalous increase to volcanic forcing, which is significantly correlated with the precipitation reduction ($r = -0.68$). It is found that most CMIP5 models underestimate the change in vertical motion as well. These results suggest that CMIP5 models' weaker response in latent heat flux and 500 hPa vertical motion could be critical factors for their underestimation of precipitation reduction.

In order to further understand mechanisms associated with the precipitation reduction, we examine monsoon circulation weakening as suggested by previous studies (Cao et al. 2012). By comparing precipitation minus evaporation ($P - E$) over land and ocean, we find that monsoon circulation decreases in both observations and CMIP5 models. It is also found that models generally underestimate this dynamic response, which is closely related to vertical motion. We also examine chain of responses with running averaged precipitation and latent heat following Joseph and Zeng (2011), comparing results over land and ocean. It is found that latent heat

flux is a response to precipitation reduction in land while precipitation is a response to latent heat flux over ocean. This indicates that monsoon type flow and air moisture change to volcanic forcing is important in precipitation response over the land. In opposite, latent heat or evaporation response has crucial role in precipitation over the ocean.

Based on our analysis results, a schematic of climate responses over global land to volcanic eruptions is constructed in Fig. 9. Reduction of shortwave (downward) radiation due to volcanic eruptions will induce reduction in surface temperature and moisture. This direct impact can be regarded as a thermodynamic response in line with the Clausius–Clapeyron relation, which can be well reproduced by CMIP5 models. There are indirect responses associated with atmospheric circulation changes, which involve vertical motion reduction and monsoon circulation weakening ($P - E$). This dynamic change seems to mainly explain the precipitation reduction over land and the latent heat increase (downward direction: decrease in evaporation from surface to atmosphere). All of these dynamic responses are found to be underestimated by CMIP5 models. What factors or processes connect thermodynamic responses to dynamic responses (marked as dashed arrows) remains unclear, particularly in models.

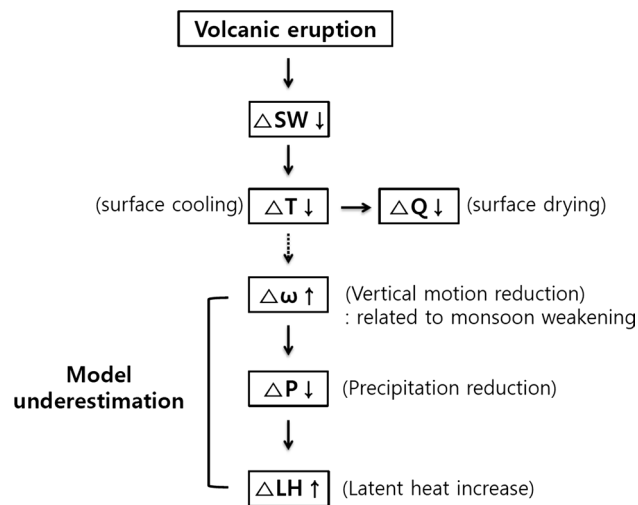


Fig. 9 Schematic of climate responses to volcanic eruptions: SW (shortwave radiation), T (surface air temperature), Q (surface specific humidity), ω (500 hPa vertical motion, positive: downward motion), P (precipitation), and LH (latent heat flux, downward direction). *Solid arrows* represent the order of responses, and a *dashed arrow* depicts unclear physical processes responsible for the change. The model underestimation indicates weaker responses in CMIP5 models compared to the observed responses

There could be regional responses to volcanic forcing, which cannot be explained by our mechanism as described in Fig. 9. For example, Joseph and Zeng (2011) found that

the equatorial regions have less cooling than subtropics, although aerosols are generally more concentrated around the equator. The local warming was suggested to be associated with (1) decrease in clouds, which induces increase in the shortwave radiation reaching the surface, and (2) lower evaporation over the regions due to lower precipitation, which may lead to a local warming. Wegmann et al. (2014) also identified weaker warming over central Africa and southern Asia during boreal summers following eruptions in their model simulations. In order to check whether such local warming in the tropics exist in our models, we examine the monthly-mean responses of zonally averaged land temperature, precipitation, down-welling shortwave radiation and evaporation using ALL MMEs (Fig. 10). Results suggest that equatorial regions indeed have a less cooling than subtropics. Stronger reduction in precipitation and evaporation is seen in the equatorial regions than subtropics together with a smaller decrease in down-welling shortwave radiation. These results are generally consistent with the previous findings, supporting their arguments, but further investigation is needed to establish physical mechanisms.

Results from this study have some important implications for geoengineering based on the solar radiation management. Given apparent increasing trends in global surface temperature and extreme events, geoengineering has received attention for alternative solution to mitigate dangerous warming (Govindasamy and Caldeira 2000). Several

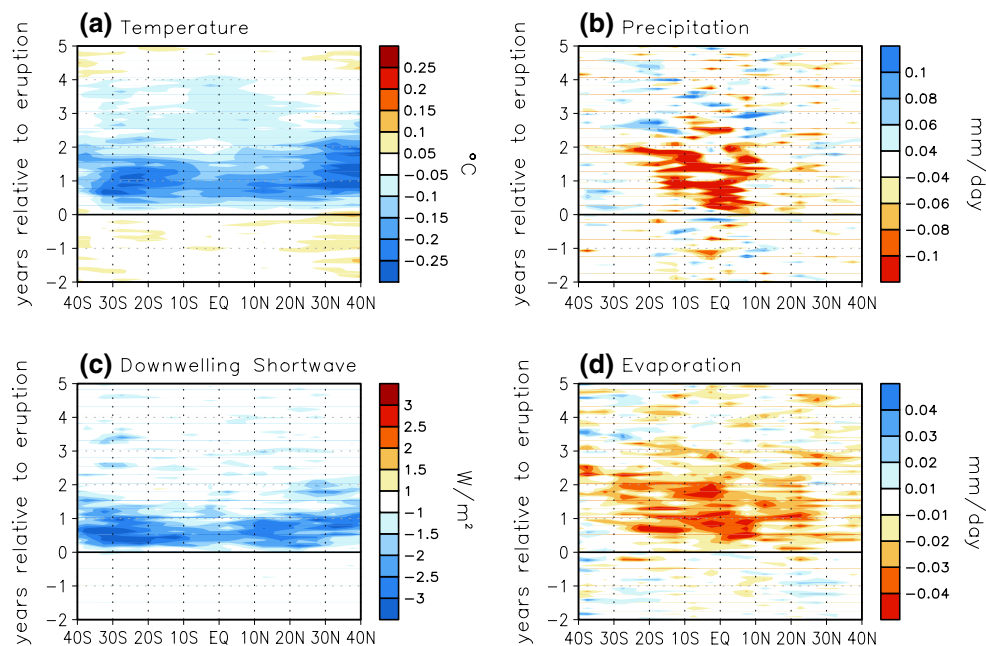


Fig. 10 Latitudinal distributions of MME ALL responses following four volcanic eruptions for zonal mean anomalies averaged over the land: **a** surface air temperature, **b** precipitation, **c** down-welling short-

wave radiation, and **d** evaporation. *Horizontal black lines* indicate the exact time of month when volcanoes erupted

studies have analyzed side effects of geoengineering with idealized experiments and suggested that artificial reduction of solar radiation can alter hydrological cycle properties, possibly increasing the risk of worldwide drought or freshwater deficiency, since the hydrological sensitivity to solar forcing is larger than to CO₂ forcing (Bala et al. 2008; Hegerl and Solomon 2009; Curry et al. 2014; Cao et al. 2015). Our study reaffirms that global climate models generally underestimate the precipitation response following volcanic forcing, which indicates that a similar model underestimation may occur to the geoengineering forcing. Therefore, thermodynamic and dynamic factors related to models' precipitation underestimation should be further investigated in the context of geoengineering. Nevertheless, it should be noted that volcanic eruption is an imperfect analog for stratospheric geoengineering since volcanic eruption is a pulse forcing while geoengineering would inject aerosols continuously and also there will be confounding effects of volcanic ash (Robock et al. 2013).

We note a few caveats in this study. First, spatio-temporal limitation of the observed precipitation datasets (e.g., New et al. 2001) and the incomplete removal of ENSO influences (Iles et al. 2013) could provide some uncertainties to our results. Although we obtain consistent results between two reanalyses, particularly for latent heat and 500 hPa vertical motion, there might remain large uncertainty in those variables (Sterl 2004; Uppala et al. 2005; Compo et al. 2011). Also, although we suggest the importance of vertical motion and monsoon circulation changes to volcanic forcing, CMIP5 models may have systematic biases in the representation of convection and monsoon climatology and variability (Flato et al. 2013), which needs to be considered more comprehensively in the future work.

Acknowledgments Authors thank Jong-Seong Kug and Dong-Hyun Cha for their comments on an early draft of this paper, and two anonymous reviewers for their constructive and clarifying comments. This work was supported by the Korea Meteorological Administration Research and Development Program under Grant KMIPA 2015–2082. The lead author was partly supported by “Human Resources Program in Energy Technology” of the Korea Institute of Energy Technology Evaluation and Planning (KETEP), granted financial resource from the Ministry of Trade, Industry & Energy, Republic of Korea (No. 20144030200460).

References

- Adams JB, Mann ME, Ammann CM (2003) Proxy evidence for an El Niño-like response to volcanic forcing. *Nature* 426:274–278
- Andres RJ, Kasgnoc AD (1998) A time-averaged inventory of subaerial volcanic sulfur emissions. *J Geophys Res Atmos* 103:25251–25261
- Bala G, Duffy PB, Taylor KE (2008) Impact of geoengineering schemes on the global hydrological cycle. *Proc Natl Acad Sci USA* 105:7664–7669
- Baran AJ, Foot JS (1994) New application of the operational sounder HIRS in determining a climatology of sulphuric acid aerosol from the Pinatubo eruption. *J Geophys Res* 99:25673–25679
- Barnes JE, Hofmann DJ (1997) Lidar measurements of stratospheric aerosol over Mauna Loa Observatory. *Geophys Res Lett* 24:1923–1926
- Bluth GJS, Rose WI, Sprod IE, Krueger AJ (1997) Stratospheric loading of sulfur from explosive volcanic eruptions. *J Geol* 105:671–683
- Cao L, Bala G, Caldeira K (2012) Climate response to changes in atmospheric carbon dioxide and solar irradiance on the time scale of day to weeks. *Environ Res Lett* 7:034015. doi:10.1088/1748-9326/7/3/034015
- Cao L, Bala G, Zheng M, Caldeira K (2015) Fast and slow climate responses to CO₂ and solar forcing: a linear multivariate regression model characterizing transient climate change. *J Geophys Res Atmos* 120:12037–12053
- Compo GP, Whitaker JS, Sardeshmukh PD et al (2011) The twentieth century reanalysis project. *Q J R Meteorol Soc* 137:1–28
- Curry CL, Sillmann J, Bronaugh D et al (2014) A multimodel examination of climate extremes in an idealized geoengineering experiment. *J Geophys Res Atmos* 119:3900–3923
- Driscoll S, Bozzo A, Gray LJ, Robock A, Stenchikov G (2012) Coupled Model Intercomparison Project 5 (CMIP5) simulations of climate following volcanic eruptions. *J Geophys Res* 117:D17105. doi:10.1029/2012JD017607
- Emile-Geay J, Seager R, Cane MA, Cook ER, Haug GH (2008) Volcanoes and ENSO over the past millennium. *J Clim* 21:3134–3148
- Fischer EM, Luterbacher J, Zorita E, Tett SFB, Casty C, Wanner H (2007) European climate response to tropical volcanic eruptions over the last half millennium. *Geophys Res Lett* 34:L05707. doi:10.1029/2006GL027992
- Flato G, Marotzke J, Abiodun B et al (2013) Evaluation of climate models. In: Stocker TF, Qin D, Plattner GK et al (eds) *Climate Change 2013: The Physical Science Basis. Contribution of Working Group I to the Fifth Assessment Report of the Intergovernmental Panel on Climate Change*. Cambridge University Press, Cambridge
- Gillett NP, Weaver AJ, Zwiers FW, Wehner MF (2004) Detection of volcanic influence on global precipitation. *Geophys Res Lett* 31:L12217. doi:10.1029/2004GL020044
- Govindasamy B, Caldeira K (2000) Geoengineering Earth's radiation balance to mitigate CO₂-induced climate change. *Geophys Res Lett* 27:2141–2144
- Gu G, Adler RF, Huffman GJ, Curtis S (2007) Tropical rainfall variability on interannual-to-interdecadal and longer time scales derived from the GPCP monthly product. *J Clim* 20:4033–4046
- Halpert MS, Ropelewski CF (1992) Surface temperature patterns associated with the Southern Oscillation. *J Clim* 5:577–593
- Hegerl GC, Solomon S (2009) Risks of climate engineering. *Science* 325:955–956
- Hegerl G, Luterbacher J, González-Rouco F, Tett SFB, Crowley T, Xoplaki E (2011) Influence on human and natural forcing on European seasonal temperatures. *Nat Geosci* 4:99–103
- Iles CE, Hegerl GC (2014) The global precipitation response to volcanic eruptions in the CMIP5 models. *Environ Res Lett* 9:104012. doi:10.1088/1748-9326/9/10/104012
- Iles CE, Hegerl GC (2015) Systematic change in global patterns of streamflow following volcanic eruptions. *Nat Geosci* 8:838–842
- Iles CE, Hegerl GC, Schurer AP, Zhang X (2013) The effect of volcanic eruptions on global precipitation. *J Geophys Res Atmos* 118:8770–8786
- Jones PD, Lister DH, Osborn TJ, Harpham C, Salmon M, Morice CP (2012) Hemispheric and large-scale land-surface air temperature variations: an extensive revision and an update to 2010. *J Geophys Res* 117:D05127. doi:10.1029/2011JD017139

- Joseph R, Zeng N (2011) Seasonally modulated tropical drought induced by volcanic aerosol. *J Clim* 24:2045–2060
- Kennedy JJ, Rayner NA, Smith RO, Parker DE, Saunby M (2011a) Reassessing biases and other uncertainties in sea-surface temperature observations measured in situ since 1850, part 1: Measurement and sampling uncertainties. *J Geophys Res* 116:D14103. doi:[10.1029/2010JD015218](https://doi.org/10.1029/2010JD015218)
- Kennedy JJ, Rayner NA, Smith RO, Parker DE, Saunby M (2011b) Reassessing biases and other uncertainties in sea-surface temperature observations measured in situ since 1850, part 2: biases and homogenization. *J Geophys Res* 116:D14104. doi:[10.1029/2010JD015220](https://doi.org/10.1029/2010JD015220)
- Kirchner I, Stenchikov GL, Graf HF, Robock A, Autuna JC (1999) Climate model simulation of winter warming and summer cooling following the 1991 Mount Pinatubo volcanic eruption. *J Geophys Res* 104:19039–19055
- Kodera K (1994) Influence of volcanic eruptions on the troposphere through stratospheric dynamical processes in the Northern Hemisphere winter. *J Geophys Res* 99:1273–1282
- Lambert A, Grainger RG, Remedios JJ, Rodgers CD, Corney M, Taylor FW (1993) Measurements of the evolution of the Mt. Pinatubo aerosol cloud by ISAMS. *Geophys Res Lett* 20:1287–1290
- Liu C, Allan RP, Huffman GJ (2012) Co-variation of temperature and precipitation in CMIP5 models and satellite observations. *Geophys Res Lett* 39:L13803. doi:[10.1029/2012GL052093](https://doi.org/10.1029/2012GL052093)
- Maher N, McGregor S, England MH, Gupta AS (2015) Effects of volcanism on tropical variability. *Geophys Res Lett* 42:6024–6033
- Mann ME, Cane MA, Zebiak SE, Clement A (2005) Volcanic and solar forcing of the tropical pacific over the past 1000 years. *J Clim* 18:447–456
- New M, Todd M, Hulme M, Jonse P (2001) Precipitation measurements and trends in the twentieth century. *Int J Climatol* 21:1889–1922
- Peng Y, Shen C, Wang WC, Xu Y (2010) Response of summer precipitation over eastern China to large volcanic eruptions. *J Clim* 23:818–824
- Peterson TC, Vose RS (1997) An overview of the global historical climatology network temperature database. *Bull Am Meteorol Soc* 78:2837–2849
- Robock A (2000) Volcanic eruptions and climate. *Rev Geophys* 38:191–219
- Robock A, Mao J (1995) The volcanic signal in surface temperature observations. *J Clim* 8:1086–1103
- Robock A, MacMartin DG, Duren R, Christensen MW (2013) Studying geoengineering with natural and anthropogenic analogs. *Clim Change* 121:445–458
- Santer BD, Wigley TML, Doutriaux C, Boyle JS, Hansen JE, Jones PD, Meehl GA, Roeckner E, Sengupta S, Taylor KE (2001) Accounting for the effects of volcanoes and ENSO in comparisons of modeled and observed temperature trends. *J Geophys Res Atmos* 106:28033–28059
- Santer BD, Bonfils C, Painter JF et al (2014) Volcanic contribution to decadal changes in tropospheric temperature. *Nat Geosci* 7:185–189
- Self S, Rampino MR, Zhao J, Katz MG (1997) Volcanic aerosol perturbations and strong El Niño events: no general correlation. *Geophys Res Lett* 24:1247–1250
- Sterl A (2004) On the (in) homogeneity of reanalysis products. *J Clim* 17:3866–3873
- Stothers RB (2001) Major optical depth perturbations to the stratosphere from volcanic eruptions: stellar extinction period, 1961–1978. *J Geophys Res* 106:2993–3003
- Taylor KE, Stouffer RJ, Meehl GA (2012) An overview of CMIP5 and the experiment design. *Bull Am Meteorol Soc* 93:485–498
- Trenberth KE, Dai A (2007) Effects of Mount Pinatubo volcanic eruption on the hydrological cycle as an analog of geoengineering. *Geophys Res Lett* 34:L15702. doi:[10.1029/2007GL030524](https://doi.org/10.1029/2007GL030524)
- Trenberth KE, Fasullo JT, Mackaro J (2011) Atmospheric moisture transports from ocean to land and global energy flows in reanalyses. *J Clim* 24:4907–4924
- Trepte CR, Hitchman MH (1992) Tropical stratospheric circulation deduced from satellite aerosol data. *Nature* 355:626–628
- Uppala SM, Kållberg PW, Simmons AJ et al (2005) The ERA-40 reanalysis. *Q J R Meteorol Soc* 131:2961–3012
- Wegmann M, Bronnimann S, Bhend J, Franke J, Folini D, Wild M, Luterbacher J (2014) Volcanic influence on European summer precipitation through monsoons: possible cause for “Years without Summer”. *J Clim* 27:3683–3691